FLOW AND ICE ACCRETION SIMULATION AROUND MULTIPLE AIRFOILS

D.F. Volkers   and
Senior Specialist
Aerodynamics
Fokker Aircraft B.V.
Amsterdam
The Netherlands

K.M.J. de Cock   and
Specialist Computational
Aerodynamics
NLR
Amsterdam
The Netherlands

N. van Lipzig
Trainee at Fokker Aircraft
Graduated in Physics at
Eindhoven University of
Technology
The Netherlands

Abstract

Simulation of ice accretion and the flow around iced multiple airfoils is of great industrial importance.
A short description of the flow and ice accretion simulation methods, currently under development at the National Aerospace Laboratory NLR and Fokker, is given. Furthermore a so-called pole's method is described which accounts for the effect of large roughness on the boundary layer development.
Computational results are compared with results from wind tunnel tests.
More study is required to improve the ice accretion method for accurate estimation of the heat fluxes that play a role in the heat balance.
To improve the prediction of the degradation of the aerodynamic characteristics of iced multiple airfoils and to ease the computations a Fully Automated Navier Stokes code is under development at the NLR.

List of Symbols

text	description	unit
AR	aspect ratio of a triangle	-
b	dimensionless center-to-center roughness element spacing	-
B	influence factor accounting blockage effect of roughness elements in normal to streamwise direction	-
c	chord	m
cd_1	form drag coefficient of roughness elements	
c_f	wall friction coefficient	-
Cp_{loc}	local pressure coefficient	-
Cp_h	specific heat of air at constant pressure (1006.)	J/kgK
Cp_{hw}	specific heat of water (4180.)	J/kgK
d	dimensionless roughness element (pole) diameter	-
e_s	vapor pressure of water at 0°C (610.)	Pa
e_∞	vapor pressure in free stream	Pa
f	roughness correction factor for h_c	-
f	influence factor accounting blockage effect of roughness elements in streamwise direction	-
F_{drop}	mass flux of impinging droplets	kg/m²s
F_{freez}	mass flux of freezing water	kg/m²s
F_{runbi}	mass flux of runback water into element	kg/m²s
F_{runbo}	mass flux of runback water out of element	kg/m²s
h	dimensionless stepheight	-
h_c	heat transfer coefficient	W/m²K
h_{fusn}	latent heat of fusion of water ($3.34 \cdot 10^5$)	J/kg
H_{max}	shape factor, max = 2.8	-
k	thermal conductivity of air (.0242)	W/mK
k	dimensionless roughness height	-
k_s	dimensionless equivalent sand grain roughness	-
LWC	liquid water content	kg/m³
L_v	latent heat of vaporization of water ($22.6 \cdot 10^5$)	J/kg
n	freezing fraction	-
P_{loc}	local static pressure	Pa
Pr	Prandtl number of air (.71)	-
P_∞	free stream pressure	Pa
Q_{conv}	convection heat flow	W/m²
Q_{evap}	evaporation heat flow	W/m²
Q_{freez}	freezing heat flow	W/m²
Q_{warm}	droplet warming heat flow	W/m²
r	recovery factor (.89)	-
Re_c	Reynolds number based on chord length	-
Re_s	Reynolds number based on streamwise coordinate	-
RH	relative humidity	%
s	dimensionless streamwise coordinate	-
T_{loc}	local flow temperature	K
T_{runbi}	temperature of runback water into element	K
T_{runbo}	temperature of runback water out of element	K
T_{wall}	wall temperature	K
T_∞	free stream temperature	K
U_{loc}	local flow velocity	m/s
U_∞	free stream flow velocity	m/s
x	chordwise distance measured from leading edge	m
α	angle of attack	-
$\mathcal{L}$	Lewis number (.915)	-
ρ_{ice}	density of ice	kg/m³
θ	dimensionless momentum thickness	-
υ	kinematic viscosity of air	m²/s

Introduction

Flight in icing conditions with failed (or switched-off) anti- or de-icing systems is an important certification item. The effect of ice accretion on aircraft performance depends on the shape, location and texture of the ice accretion.

The Joint Aviation Requirements JAR-25 for Large Aeroplanes[1] present in ACJ 25-1419 interpretations and an acceptable means of compliance.

For those parts of the airframe where the accretion of ice under the conditions of Appendix C of JAR-25 is likely to have an adverse effect on the airworthiness of the aeroplane, tests should be performed to show that the safety of the aeroplane is not adversely affected.

It is accepted that flight tests are done with simulated ice shapes to demonstrate the safety of the aircraft. Tests in natural icing conditions have to be performed to demonstrate the effectiveness of the ice protection system and to judge the tests with simulated ice shapes for their acceptibility.

In general the tests with simulated ice shapes are much easier to schedule than the tests in natural icing conditions.

However, one must be convinced that the adopted ice shape, texture and locations of the ice are representative for the aircraft in icing conditions. Furthermore it is of importance that the predicted aerodynamic degradation is in agreement with test data.

A description is given of a code for ice accretion computation, followed by the description of a 2-D unstructured Euler code for calculation of the pressure distribution on multiple airfoils. Also a description is given of a 2-D integral boundary layer code which accounts for large roughness (larger than the displacement thickness) and turbulent separation bubbles.

Results obtained from applications of the codes are discussed and compared with measured data.

Description of computational method

General

The purpose of ice accretion computations is to aid the selection of a suitable ice shape for the simulated ice tests described in ref. 2.

Moreover the results are used to evaluate the flight safety aspects of the aircraft fitted with simulated ice accretion, before the actual flight tests take place. Therefore, not only the ice shape, but also its effect on aerodynamic characteristics must be evaluated.

Ice accretion computation

The ice-shape prediction method ICE is based on physical expressions. It can be applied to a wide range of icing conditions. In particular, rime ice shapes are generated as a limiting case of glaze ice shapes with decreasing temperature and decreasing liquid water content (LWC).

Rime ice occurs at very low temperatures (below 20°C approx.) and low values of LWC. In these conditions the dissipation of heat is sufficient to freeze all the impinging water immediately on impact. It displays itself as a smooth, streamlined shape causing a modest aerodynamic penalty only.

Due to air trapped in it, rime ice is porous, is white, and has a relatively low density of about 880 kg/m^3. Glaze ice occurs at higher temperatures. Heat transport is insufficient to freeze all the impinging droplets. As a consequence, water at 0°C flows along the ice surface (due to shear stress) and either freezes further downstream or eventually leaves the trailing edge. The exact behavior of this type of water flow has been investigated only in recent years, and its importance for the final ice shapes is now acknowledged. However, a theory or empirical expression suitable for direct implementation in a code is not yet available. The present program resorts to a simplified water-film model. The external appearance of glaze ice is characterized by the formation of two horns, one above and one below the stagnation area. This is what the aircraft operator fears most, since it results in an appreciable increase in drag and loss of maximum lift. The surface of glaze ice is rough due to the surface water. The ice itself is transparent.

ICE uses a time-stepping procedure to compute the ice accretion on an airfoil layer by layer in a quasi-steady way, assuming constant conditions during the growth of each layer. The calculation procedure for each layer can be broken down into four major steps:
- calculation of flowfield
- calculation of droplet trajectories
- solution of the heat- and massbalance
- definition of new airfoil shape

The flowfield calculation yields the input for droplet trajectory calculations and produces variables required in the heat and mass balance module. The droplet trajectory module calculates the water catch distribution and catching angles of homogeneous clouds with discrete, but multiple, droplet sizes. By performing the heat and mass balance on the caught flowfield, the amount and position of freezing water is solved. Finally the ice is added to the profile. These four steps will be discussed in the following paragraphs.

Flowfield and boundary layer parameters

The flowfield is calculated in the program ICE using the program FLXPAN. This is a first-order, incompressible (and inviscid) panel method, which uses linear vorticity distributions on straight panels and solves the stream function in the panel midpoints.
There is no compressibility correction.
The Kutta condition is enforced by requiring equal pressures on the upper and lower surface near the trailing edge.
The local velocity, flow temperature and turbulent heat transfer coefficient are calculated in the panel midpoints from

$$U_{loc} = U_\infty \sqrt{1 - C_{p_{loc}}}$$

$$T_{loc} = T_\infty + \frac{U_\infty^2 \, C_{p_{loc}}}{2 \, C_{p_h}}$$

$$h_c = f \cdot .0296 \cdot k \cdot Pr^{1/3} \cdot \frac{Re_s^{4/5}}{s}$$

The heat transfer coefficient h_c is the most important parameter in the ice accretion calculation.
Comparison of measured ice shapes with those calculated show discrepancies in ice-shapes and freezing fractions which indicate that too low values of h_c have been used in the computations. This is not surprising in view of the fact that h_c was derived for a flow along smooth surfaces. In order to correct for roughness the factor f has boldly been introduced and sized for best agreement of calculated and measured ice shapes, which has resulted in f=2.0.
The heat transfer coefficient for stagnation flow is used as a lower boundary for the value of h_c in the stagnation area.

$$h_{c_{stag}} = \frac{1}{2} \cdot k \sqrt{\frac{(dU/ds)_{stag}}{v}}$$

Droplet trajectories and impingement parameters

Droplet trajectories are calculated within ICE by running a separate routine. This routine solves the equations of motion for a droplet. Droplets of prescribed diameter, assumed spherical and solid, are released 1.5 chord lengths in front of the airfoil leading edge with a velocity equal to the local air velocity. The droplets follow their path until impact on the airfoil.
The catching efficiency is calculated in every point of droplet impact.

Heat and Mass Balance

With the flowfield and the impingement established, a heat and mass balance is performed which yields an ice accretion rate as a function of arc length along the airfoil surface. The ice accretion process is modelled as in figs. 1 and 2. The elements in which the heat and mass balance are performed are taken equal to the airfoil panels.
Of all the possible contributions to heat transfer only the dominant ones are taken into account by ICE:
  - convection (adiabatic cooling and frictional heating)
  - evaporation
  - latent heat of freezing
  - droplet warming
  - runback water warming
And in the massbalance:
  - droplet impingement
  - runback inflow/outflow
  - water freezing

Water droplets that impact on an element (panel) either freeze immediately at the point of impact or run back along the airfoil surface into the next downstream element (or into both neighboring elements if the stagnation point happens to be on this element). If there is insufficient outflow of heat to freeze all of the impacting water, it is assumed that there is a thin, continuous film of water that covers the ice. This implies that evaporation will act on the entire element area. This waterfilm-model has been used in most other analytic ice-accretion codes as well[3][4]. However, experiments[5] have shown that the actual ice-accretion process is different in most of the accretion region so that this model is of questionable validity.
The terms that are accounted for in ICE are implemented by means of the following formulae:
- Convection heat flow (adiabatic cooling and frictional heating)

$$Q_{conv} = h_c \left(T_{wall} - T_{loc} - r \frac{U_{loc}^2}{2 \, C_{p_h}} \right)$$

$$T_{wall} = 0^\circ C$$

- Evaporation heat flow

$$Q_{evap} = h_c \frac{.622 \, L_v}{C_{p_h} Pr^{2/3} P_{loc}} \{ e_s \frac{T_{loc}}{T_{wall}} - e_\infty \frac{P_{loc}}{P_\infty} \}$$

The water vapor pressure in the free stream, e_∞, is calculated as the product of the user-specified relative humidity and the saturation pressure at free-stream static temperature.

- Freezing heat flow

$$Q_{freez} = F_{freez} \cdot h_{fusn}$$

- Droplet and runback water warming

$$Q_{warm} = \{F_{drop} \cdot (T_{runbo} - T_\infty)$$
$$+ F_{runbi} \cdot (T_{runbo} - T_{runbi})\} \cdot Cp_{hw}$$

The heat- and massbalances read:

$$Q_{conv} + Q_{evap} + Q_{warm} = Q_{freez}$$

$$F_{drop} + F_{runbi} = F_{runbo} + F_{freez}$$

These two equations solve for the *three* unknowns F_{freez}, F_{runbo} and T_{runbo}. This is possible as one of them is always fixed in any of three possible icing regimes, i.e. they are not truly independent. Introducing the freezing fraction (the ratio of water freezing in the element to that entering it)

$$n = \frac{F_{freez}}{F_{drop} + F_{runbi}}$$

the following three cases can be distinguished:

surface	wet	wet	dry
accretion	no	yes	yes
type	-	glaze	rime
freezing frac.	$n=0$	$0<n<1$	$n=1$
constant	$F_{freez}=0$	$T_{runbo}=0$	$F_{runbo}=0$
solve for	F_{runbo},	F_{freez}	F_{freez}
	T_{runbo}	F_{runbo}	T_{runbo}

The value of n is of course also the outcome of the two balances. An iterative procedure is used to solve for n. This is done by assuming $T_{runbo}=0$ °C (i.e. $0<n<1$) and then selecting the appropriate formulae if n turns out to be negative or larger than one.

Accretion

The accretion rates found from the heat- and mass-balance are used to define the new iced-airfoil geometry. In this process airfoil contour points are shifted to their new positions on the outer surface of the ice layer. Finally the new airfoil contour is repaneled to prevent formation of an undesirable panel distribution during subsequent time-steps.
The amount of water frozen is simply laid out over the curved surface, without any indication on how the terms in the heat balance evolve during a single time-step. The ice is applied in the direction of the panels bisector. Thus, the ice is assumed to grow normal to the surface.
The program requires a time step. Here the time is

entered that will be used in every subsequent time step of the ice accretion process.
The time step should be chosen such that the thickness of the accreted ice layer is on an average 0.5% chord for a good compromise between accuracy and computing time. A first estimate is given by

$$\text{time step} = \frac{.005 \cdot \rho_{ice} \cdot \text{chord}}{U_\infty \cdot \text{LWC}}$$

Description of 2-D unstructured Euler code

An unstructured grid is generated around the multiple airfoils with and without ice accretion, using the grid generator of the FANS[6] code. The unstructured grid approach is chosen because it offers a great flexibility with respect to automatic grid generation around complex shapes, requiring a minimum of user-defined input parameters. Characteristics of the grids used are:

Config.	nodes	triangles	max AR	% nodes on solid wall
Flap IN IS1S	9909	19220	4.7	5.5
Flap 18 clean	11881	23024	6.1	5.8
Flap 18 IS1S	14252	27652	13.2	5.7

A detail of this grid around the ice accretion is given in fig. 3. On these grids, the two dimensional steady Euler equations are solved. Characteristics of the Euler solver are:
- finite volume discretization of the physical space,
- integration to steady state by a multi-grid version of the multi-stage Jacobi relaxation scheme,
- upwind flux difference splitting of the fluxes and,
- second order accuracy by the defect correction and MUSCL technique.

The Euler solver yields the static density, velocity vector and static pressure around and on the multiple airfoils. From this data the pressure coefficient distribution on the multiple airfoils can be calculated. Due to the numerical viscosity linked to the discretised Euler equations, vortices originating from the sharp edge of the ice accretion can be simulated, see fig. 4.

Description of 2-D integral boundary layer code

The effect of ice accretion on the drag coefficient is computed using an integral boundary layer method. The input for said method consists of:
pressure distribution, roughness distributions, location of bubble (begin and end coordinates), Reynolds number based on chord length and Mach number.

Pressure distribution:
On an airfoil with ice accretion a pressure distribution must be available.
In this study the pressure distribution was obtained from a combination of measured data on the 2-D model, Model 5-6 and data computed with the Euler program (nose part with ice accretion).
A Fully Automated (automatic grid generation) Navier Stokes code is under development at NLR to deal with this type of bubbles and bubbles which occur typically on multi-element airfoils i.e. slat cove and flap shroud.

Boundary layer:
For the laminar part of the boundary layer Thwaite's[7] method is used.
For a smooth airfoil the transition location is obtained with Michel's[7] criterion.
The turbulent boundary layer is analyzed using Head's[7] method.
For the closing formula the skin friction coefficient according to Ludwig-Tillman[7] is used.
On airfoils with ice accretion the surface is normally not smooth.
For cases where the roughness is smaller than the boundary layer displacement thickness (computed at the previous station) the following formula is used to calculate the skin friction coefficient:

$$\sqrt{\frac{2}{c_f}} = 5.91 \, \log\left(\frac{\theta}{k_s}\sqrt{\frac{2}{c_f}}\right) + 6.91 \; ,$$

obtained from ref.8.
This relationship between skin friction coefficient c_f, equivalent sand grain roughness k_s and the momentum thickness is based on pipe flow data of Nikuradse and turbulent flow over a rough plate by Granville.
The main difficulty in validating this method is the determination of the equivalent sand grain roughness.
At Fokker "off the shelf" sand paper was used and fixed on the wind tunnel model.
Using the roughness height k (as indicated by the grit number on the sand paper) and an estimated concentration, the equivalent sand grain roughness can be obtained.
For cases where the roughness is larger than the displacement thickness (computed at the previous station) a so-called "pole's" method is used in combination with Head's method.
Two modifications are made.
1. At each pole an increment in momentum thickness is added to the computed momentum thickness

$$\Delta\theta = cd_1 \cdot \frac{d}{b} \cdot k \cdot \left(\frac{U_r}{U_{loc}}\right)^2$$

using cd_1 = drag coefficient for a pole (=0.4),
  d = dimensionless diameter of the pole,
  b = dimensionless pole center to center spacing.
The pole center to center spacing is obtained from the concentration and the diameter of the poles

$$b = d \, /\sqrt{\text{concentration}} \; ,$$

k = dimensionless height of the pole,

$$\left(\frac{U_r}{U_{loc}}\right) = 0.85 = \text{average velocity felt by pole}$$

relative to local velocity.

2. Because there is also friction between the poles and the air, the friction coefficient used in Head's method is modified:

$$c_f = c_{f\,smooth} + \frac{1}{2}\frac{cd_1 \cdot d \cdot k}{b^2}\left(\frac{U_r}{U_{loc}}\right)^2\frac{f}{B}$$

using $f = \left[1-\frac{d}{b}\right]/B$

and $B = 1-\frac{\pi}{4}\frac{d^2}{b^2}$

Factor $\left[1-\frac{d}{b}\right]$ accounts for the blockage effect due to roughness-elements in streamwise direction. Factor B accounts for the blockage effect in the spanwise direction.

Turbulent separation bubble:
Two dimensional flows identify separation of flow by the inception of reverse flow, the separation point being the forward boundary of a vortex sheet embedded within a separated region.
This leads to negative values of the friction coefficient in the bubble region. Figure 4 shows an example of the computed velocity components in such a bubble.
Within the integral method, the turbulent separation bubble is computed using:

$$\frac{d\theta}{ds} = -(H_{max}+2)\frac{\theta}{U_{loc}}\frac{dU_{loc}}{ds}$$

H_{max} = 2.8 is used.
Moreover a jump in θ is applied at the beginning of the bubble using the relation:

851

$$\Delta\theta = \frac{cd_h \cdot h}{2} \cdot \left(\frac{U_{loc}}{U_\infty}\right)^2$$

with cd_h = .022 according to ref. 9 (backward facing step) and h = dimensionless step height at the beginning of the bubble.
The beginning of the bubble is at the sharp ice edge (see fig. 4) and the end is obtained from oil flow visualization tests.

Downstream of the reattachment point the turbulent boundary layer is computed (using the previously described Head's method including roughness/pole's if necessary) onto the trailing edge of the airfoil element or until separation is found.
The Squire-and-Young formula[7] is used to compute the drag coefficient on upper and lower surface.

Description of tests

Certification tests

Reference 2 presents a discussion of the certification process for the Fokker 50 and Fokker 100.
Figure 5 shows the sharp ice shape on the Fokker 100 wing leading edge, with a clean upper surface just downstream of the ice ridge.
Figure 6 shows the rough texture and the extent of the glaze ice on the lower surface of the Fokker 50 wing.
Some of the characteristics of these ice shapes are found in the configuration adopted for the wind tunnel tests.
In Appendix C of JAR-25 a distinction is made between Intermittent Maximum icing conditions and Continuous Maximum icing conditions.
Based on statistical data relations are shown between liquid water content, droplet diameter, air temperature, pressure altitude and cloud horizontal extent.
The Intermittent Maximum icing conditions are characterized by high liquid water content and small cloud horizontal extent. These conditions are usually considered in the safety analysis of a failed or delayed activated de- or anti-icing system.
The Continuous Maximum icing conditions are characterized by low liquid water content and large cloud horizontal extent.
The shape of the ice accreted in both icing conditions is totally different, as will be shown.
Another important parameter in the ice accretion is the relative humidity.
During a test in an icing tunnel it was found that the relative humidity varied between 54 % and 96 %.
In flight icing conditions the relative humidity varies

from more than 100% inside the cloud to a low value outside the cloud. For instance the down draft just outside a cumulus cloud has relatively dry air.
It is remarkable that no information on the relative humidity is given in papers where tests in icing conditions are reported.

Selection of an ice shape for the wind tunnel test and code validation purposes

A number of possible ice shapes were computed by considering the following flight conditions in Intermittent Maximum icing conditions:
- Airspeed 160 kCAS (Holding of a Fokker 100 at low weight)
- Angle of attack α = 4 deg and the wingtip airfoil chord = 1.26 m is assumed.
- Flaps and undercarriage retracted.
- Flight altitude 10,000 ft (FL100)
- Total icing time follows from ACJ 25-1419 in which three clouds of 5 km horizontal extent with intermittent maximum icing conditions are specified.
- The LWC is also obtained from ACJ 25.1419. A mean droplet diameter of 20μm is considered and the LWC was determined for three temperatures, i.e. ISA, ISA-10 and ISA-20.
- The ambient pressure used in the computations was .69 bar at 10,000 ft.

In all of the computations the airfoil surface acts as an adiabatic wall, i.e. no heat exchange between airfoil skin and air/ice is taken into account.
In reality the wing skin can act as a heater or a cooler, depending on the history of the flight before the icing encounter.

Figures 7 thru 10 show examples of the various ice shapes that were computed based on the afore-mentioned conditions.
Comparing figure 7 with figure 8 shows the large effect of relative humidity in this condition.
Because the LWC and the temperature are relatively high, the ice will freeze over a large area on upper and lower surface. In figure 7 the relative humidity is set at 100% and cooling due to evaporation becomes negligible.
In figure 8 the relative humidity is set at 0% and the contribution of evaporation becomes large. As a consequence, ice forms more forward on the airfoil nose.
Compared with figure 7, figures 9 and 10 show the effect of temperature variation of ISA-10, and ISA-20 respectively on the ice shape. The ice shapes concentrate more at the nose at lower temperatures.

852

Examples of ice accretion in Continuous Maximum icing conditions are shown in figures 11 and 12.
In these figures the effect of temperature is shown.
In figures 11 and 12 a succesfull attempt was made to do sufficient time steps to reach a total time of 30 minutes, which is required in ACJ 25-1419.

In most of the afore-mentioned ice shapes ice accretion is found over a large area on the lower surface.
This is also confirmed by the result shown in figure 6.
In this figure the ice accretion is shown as collected on the Fokker 50 in natural icing tests.
Figure 6 also shows the very rough texture of the ice accretion.
In said tests, flown near Bergen in Norway, the temperature varied between -4 to -10 deg Celcius, the altitude varied between 9,000 and 10,000 ft. The mean droplet diameter was equal to 25 micrometer and the liquid water content was approximately LWC = 0.3 g/m³.
Figure 5 shows the ice accretion measured on the Fokker 100 in natural icing tests.
The clean upper surface downstream of the sharp ice accretion on the nose is also found in some computations, for instance see figure 9.
The ice shape for wind tunnel test and code validation purposes was derived from figure 9.

Description of the wind tunnel test

The purpose of the test was to collect data for validation of CFD codes for the evaluation of airfoils with rough ice accretion.
The wind tunnel tests were performed in the Low Speed wind tunnel LST 3x2.25 m² of the NLR in the Noord-Oost Polder in December 1993.
The two-dimensional model, Model 5-6 was used. This model represents Wing Station 6984 of the Fokker 100.
The model chord length (flaps IN) is equal to .676 m.
The model is equipped with a row of pressure taps to measure the static pressure. Total pressures were measured in the wake (4 rakes) and in the boundary layer at x/c = .805.
Upper and lower wall blowing through slots was applied to counteract the 3-D effects caused by the tunnel wall boundary layer.
Tufts were used to check the two dimensionality of the flow near maximum lift.
The ice shapes were fitted to the nose of the model with a gap of approximately 2 mm at the location of the pressure taps.
Oil was used to visualize the flow. In the oil pattern the separation and reattachment points of the boundary layer can be traced.

The following configurations were tested.
Flaps IN: clean, IS1S, IS1R
Flaps 18:   clean and IS1R
IS1S is a smooth shape, derived from fig. 9, attached to the nose of the clean airfoil.
IS1R has the same shape as IS1S but is made rough by gluing sandpaper #36 on the surface.
Figures 13 and 14 show the various configurations.

Discussion of results

Figures 15 thru 23 present some results of the wind tunnel tests. The effect of the ice accretion on the maximum lift coefficient is large for both the flap IN and flap 18 configuration, see figures 15 and 16. For flaps IN both a smooth (IS1S) and rough (IS1R) ice shape were tested. Apparently the effect of the roughness on the loss in maximum lift coefficient is small in this case.
The roughness does, however, have a large effect on the drag coefficient at low angles of attack, see figure 17.
The roughness also has an effect on the length of the separation bubble originating at the sharp edge of the ice shape (see figure 19). Figure 20 shows an example of the results of the visualization tests with the oil-film technique.
This picture shows the large bubble ending at 30%c for the case: flap 18, IS1R, α = 3 deg.
The pressure distribution on the ice shape was not measured and instead, a part of the computed pressure distribution was used. Figure 21 shows a comparison of the measured and the computed (Euler method) pressure distributions.
The Euler results are used as indicated in figure 22.
The suction peak C_p value and the pressure distribution from the sharp ice edge onto about 5% and 15 % chord are varied as indicated in figure 22.
This variation has a large effect on the computed boundary layer development, see figure 23 and thus on drag.

In boundary layer computations the roughness on the ice shape IS1R dictated the separation bubble to be turbulent.
On the clean ice shape IS1S however it was assumed that the transition from laminar to turbulent flow occurs just downstream of the sharp edge. Variation of the transition point with only 1 to 2% chord yielded large variations in computed drag coefficient.

Conclusions

The present investigation shows that the performance degradation in terms of drag increments can be understood using the results of the boundary layer method, which accounts for large roughness (larger than the displacement thickness) and separation bubbles.

- The results of the boundary layer computations are very sensitive to details of the pressure distribution in the nose region of the iced airfoil and to the size of the separation bubble.
  The size of the separation bubble is not only a function of the ice shape and angle of attack, but also of the roughness on the ice shape.

- Until now no method is available to accurately compute the pressure distribution on an airfoil with a sharp-edged ice shape.

The method to compute ice accretion can be improved by:

- Recognition and implementation of factors that influence the texture of the ice accretion: better estimate of heat transfer coefficient is needed.

- Extension of heat balance to account for non-adiabatic skin.

- More study is required of the contribution of the evaporative cooling in the heat balance.

- Statistical data is needed with respect to the relative humidity in icing conditions. In both wind tunnel and flight tests in icing conditions the relative humidity must be measured.

References

1. Joint Aviation Requirements, Change 13, JAR-25 Appendix C, 25.1419 and ACJ 25.1419. Joint Aviation Authorities, Oct. 1989

2. J.N. Boer and J. van Hengst, 'Certification of Fokker 50 and Fokker 100 for Operation in Icing Conditions', AIAA-91-0561, 29th Aerospace Sciences Meeting, January 7-10, 1991, Reno, NV.

3. B.M. Berkowitz and J.T. Riley, 'Analytical Ice Shape Predictions for Flight in Natural Icing Conditions', NASA CR 182234.

4. J.T. Cansdale and R.W. Gent, 'Ice Accretion on Airfoils in Two-dimensional Compressible Flow - a Theoretical Model', RAE TR 82128, January 1983.

5. R.J. Hansman and S.R. Turnock, 'Investigation of Surface Water Behaviour during Glaze Ice Accretion', AIAA-88-0015, January 1988.

6. K. de Cock, 'High lift system analysis method using unstructured meshes', AGARD CP 515, 1993.

7. T. Cebeci and A.M.O. Smith, 'Calculation of Profile Drag of Airfoils at Low Mach Numbers', Journal of Aircraft, vol. 5, No. 6, Nov-Dec. 1968.

8. P.A.A. Narayana, 'An Experimental Investigation of Turbulent Boundary Layers over Smooth and Rough Surfaces', Report LR-235, Delft University of Technology, January 1977.

9. S.F. Hoerner, 'Fluid Dynamic Drag, Practical Information on Aerodynamic Drag and Hydrodynamic Resistance', Library on Congress Catalog Card Number 64-19666.
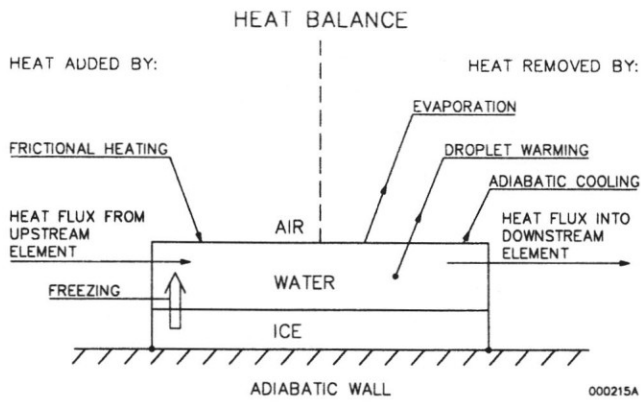
Fig. 1 Heat Balance
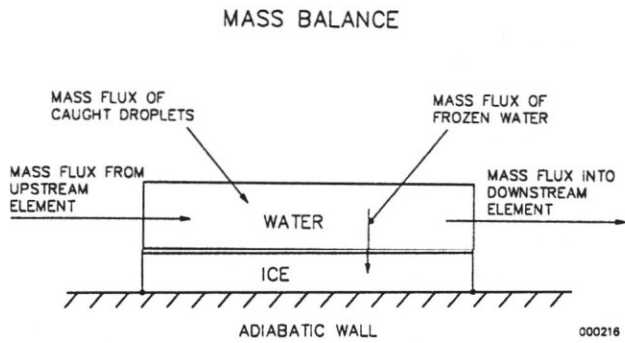
Fig. 2 Mass Balance
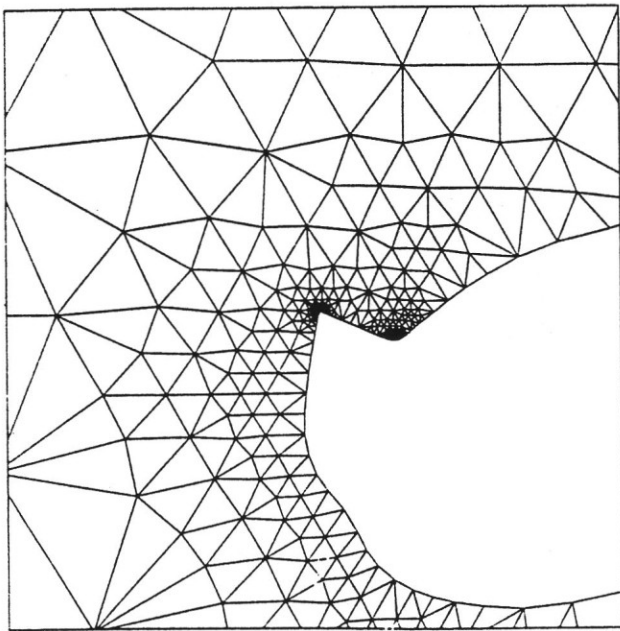
Fig. 3 First grid level around the nose
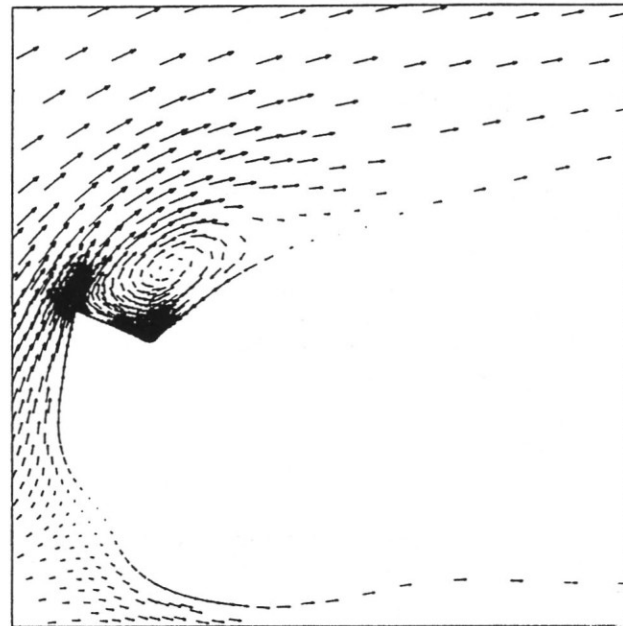
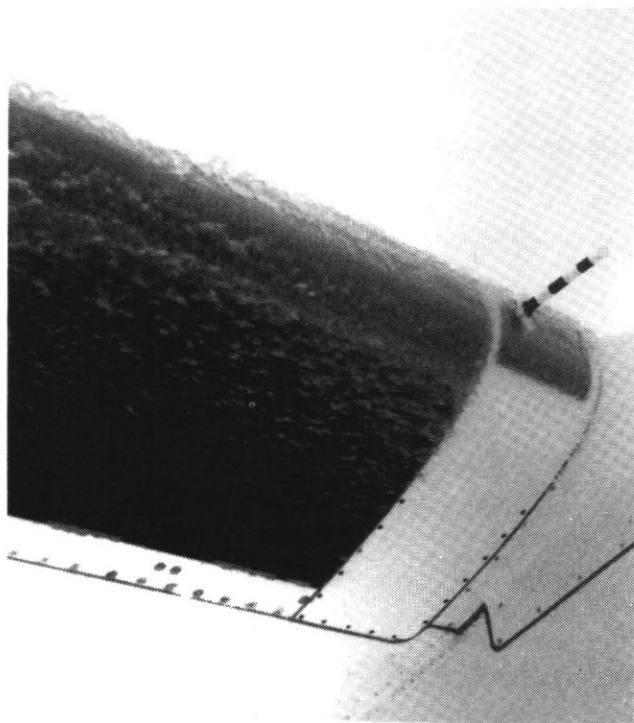Fig. 4 Velocity vector plot alpha = 6 deg, Euler

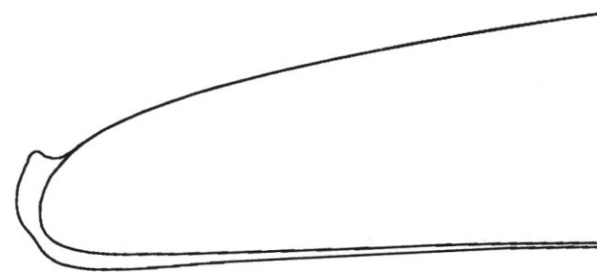Fig. 5 Fokker 100 ice accretion

Fig. 6 Fokker 50 ice accretion

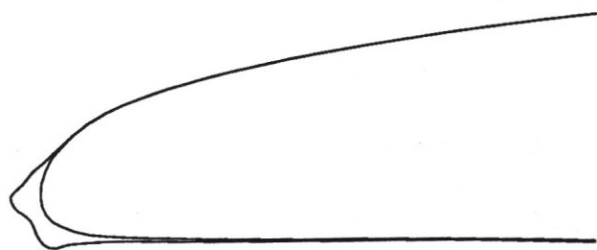Fig. 7 Computed ice accretion, Int. Max.
RH = 100%, ISA, time = 157 s

Fig. 8 Computed ice accretion, Int. Max.
RH = 0%, ISA, time = 157 s

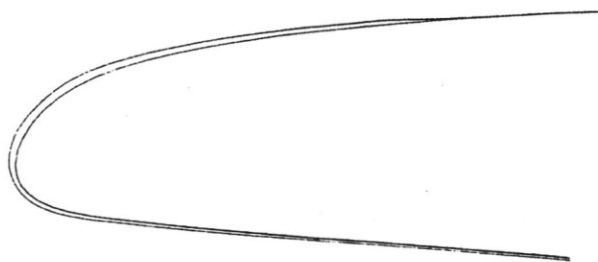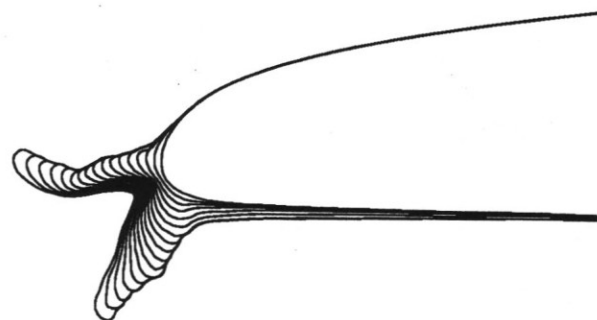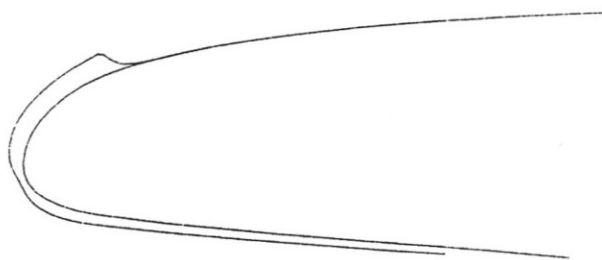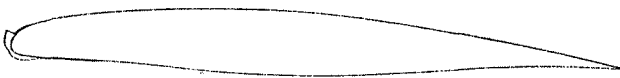Fig. 9 Computed ice accretion, Int. Max.
RH = 100%, ISA-10, time = 160 s

Fig. 10. Computed ice accretion, Int. Max.
RH = 100%, ISA-20, time = 163 s

Fig. 11 Computed ice accretion, Cont. Max.
RH = 100%, T = -12 deg C, 16 time steps of 110 s

Fig. 12 Computed ice accretion, Cont. Max.
RH = 100%, T = -22.5 deg C, 12 time steps of 150 s

Fig. 13 Configuration FLAPS IN + ice shape
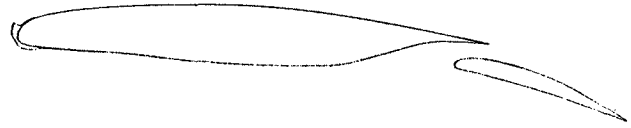
Fig. 14 Configuration FLAPS 18 deg + ice shape
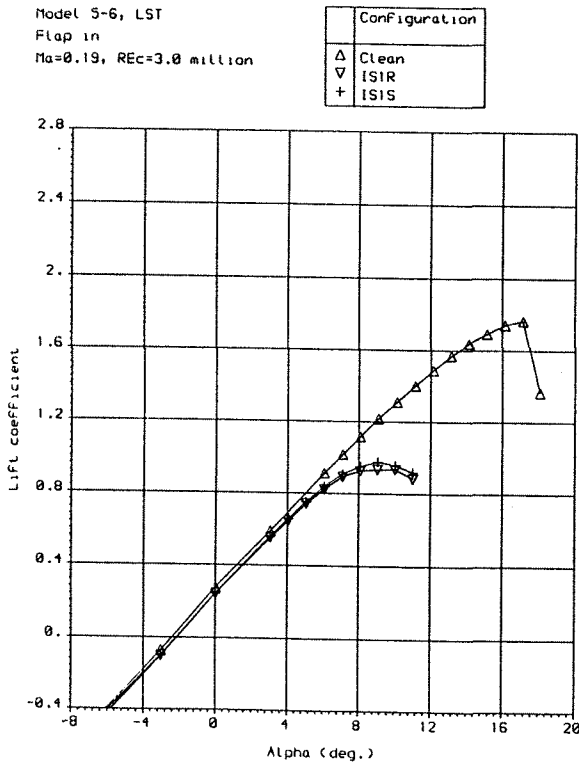
Fig. 15 Section lift curves FLAPS IN
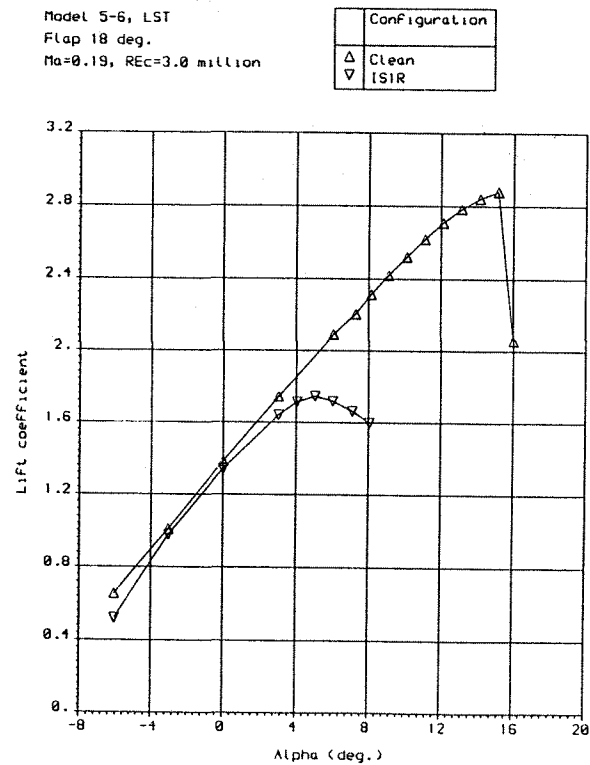
Fig. 16 Section lift curves FLAPS 18 deg
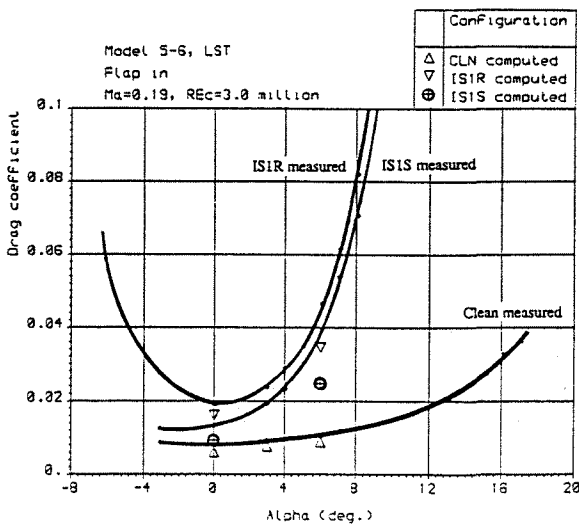
Fig. 17 Section drag curves FLAPS IN
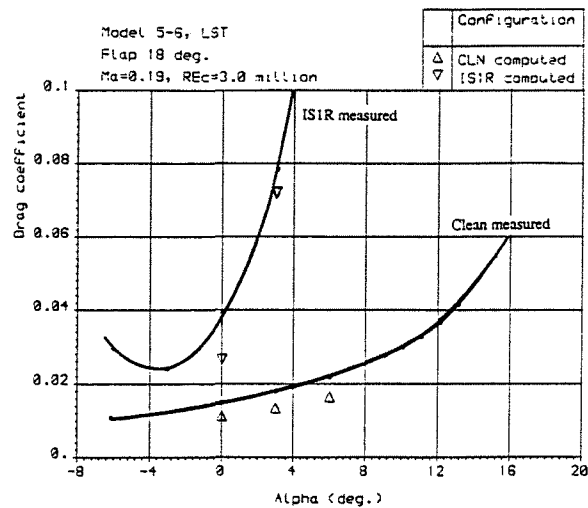
Fig. 18 Section drag curves FLAPS 18 deg

857

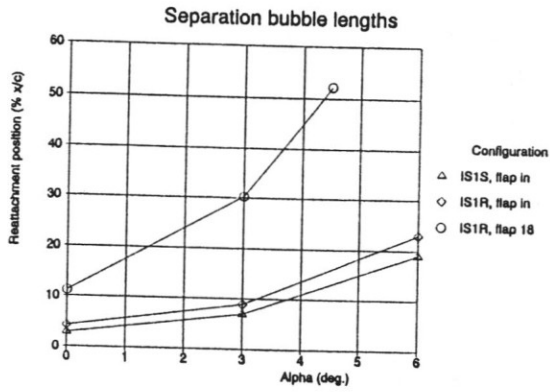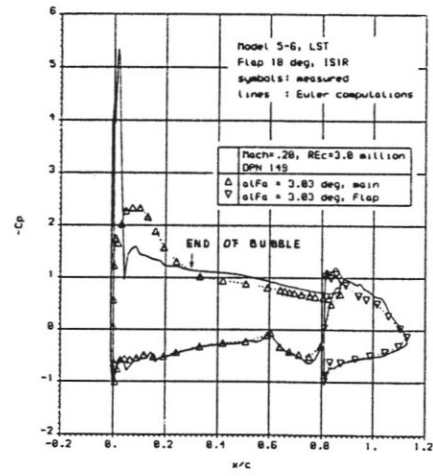Fig. 19 Measured separation bubble length

Fig. 21 Pressure Distribution FLAPS 18 deg. IS1R

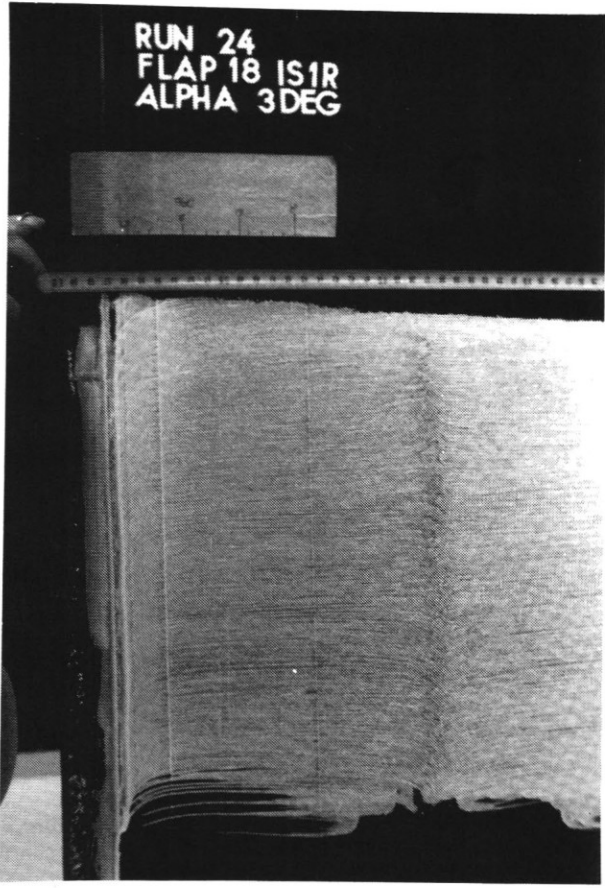Fig. 22. Detail of Pressure Distribution

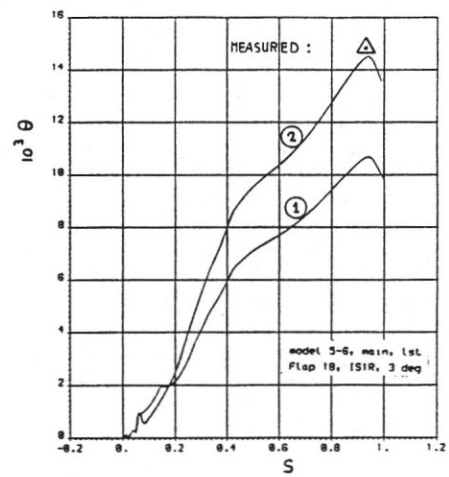Fig. 20 Oil flow visualization result

Fig. 23 Momentum loss versus streamwise coordinate